

Article

# Frequency Selective Surfaces as Reconfigurable Superstrate Applied to a Dipole Antenna for 5G NR

Thamyris da Silva Evangelista<sup>1</sup> , Juliete da Silva Souza<sup>1</sup> , Alexandre Jean René Serres<sup>1</sup> ,  
Alfredo Gomes Neto<sup>2</sup> 

<sup>1</sup>Federal University of Campina Grande, UFCG, Paraíba, Brazil, [thamyris.evangelista@ee.ufcg.edu.br](mailto:thamyris.evangelista@ee.ufcg.edu.br),  
[juliete.souza@ee.ufcg.edu.br](mailto:juliete.souza@ee.ufcg.edu.br), [alexandreserres@dee.ufcg.edu.br](mailto:alexandreserres@dee.ufcg.edu.br)

<sup>2</sup>Group of Telecommunications and Applied Electromagnetism, GTEMA Federal Institute of Paraíba, IFPB,  
Paraíba, Brazil, [alfredogomes@ifpb.edu.br](mailto:alfredogomes@ifpb.edu.br)

**Abstract**— This paper introduces a novel reconfigurable superstrate using a band-stop frequency selective surface (FSS) based on four arms star geometry. The proposed reconfigurable superstrate is applied to a dipole antenna for use in 5G NR technology with a frequency of 3.545 GHz. The study includes both simulated and experimental results which confirm the redirection of the antenna radiation pattern. The developed structure exhibits radiation in only one half-space, high polarization isolation, and a redirection of the radiation pattern up to  $\pm 55^\circ$ . The ideal cases were considered, where the ON and OFF states of the diodes were replaced by short circuits and gaps, respectively. Overall, the results demonstrate the effectiveness of the proposed FSS as a promising solution for 5G NR technology applications.

**Index Terms**— Antenna, four arms star, reconfigurable frequency selective surface, 5G NR.

## I. INTRODUCTION

The 5th generation mobile network is intended to significantly reduce communication latency, have wider network coverage depending on frequency, and enable high data transmission rates. In this context, the following stand out: Enhanced Mobile Broadband (eMBB); Massive Machine-type Communications (mMTC); Ultra-reliable Low Latency Communications (URLL); and long-range access networks, including rural applications. Regarding broader network coverage, the optimization of the radiation beam with the beamforming technique has shown promise. The 5th generation network will use a large number of antennas with multiple inputs and multiple outputs, Massive MIMO, to control the direction of propagation of the emitted radio frequency waves, which allows for better performance in connectivity and speed between the antenna and the end use [1]-[6].

In 2017, the 3rd Generation Partnership Project (3GPP), launched the 5G New Radio (NR), a new radio interface and access technology for cellular networks. The 5G NR uses two frequency bands: frequency band 1 which includes frequency bands up to 6 GHz and frequency band 2 which includes the 20-60 GHz bands. The main benefits of 5G NR will include increased capacity for wireless users, better links between users with less latency and network loss, and faster data rates [7], [8].

In Brazil, on November 23, 2021, the National Telecommunications Agency (Anatel), approved the result of the frequency auction that determined the distribution of the 5G signal, in the 700 MHz, 2.3 GHz, 3.5 GHz, and 26 GHz bands [9]. Due to the implementation of 5G networks, several researchers have been motivated to develop more efficient antennas that can improve the transmission capacity of systems by directing the electromagnetic signal, favoring better use of the spectrum, and preventing the signal from being radiated in unwanted directions [10]-[12].

In 1986, McGrath [13] was the first to introduce a microwave lens with focus and scan capabilities, connecting two patch antennas using pathways on both sides of the flat structure, forming a spatial array, called a transmitarray. Since then, the transmitarray has been the focus of several studies. It is worth mentioning that the term “transmitarray” is the conventional name given to structures that can modify the original radiation pattern of a directional antenna, such as a horn antenna, when placed at a distance sufficiently far from its aperture. The combination of the structure and the radiating source is referred to as a transmitarray antenna [14]-[17].

Pirhadi, Keshmiri, and Hakkak [18] presented a dual-band antenna using a passive FSS as a superstrate. It was possible to obtain a gain of 18 dBi at 11.25 GHz and 13.15 GHz, compared to a patch antenna, with 6 dBi. Sazegar et al. [19] used a reconfigurable FSS with beamforming steering capability. The FSS works as a band-pass filter, with a frequency centered at 12 GHz. The novelty of the work is based on the design of the FSS, composed of capacitive and inductive structures printed on a thick-film ceramic of barium strontium titanate (BST). Experiments performed report a maximum phase difference of  $121^\circ$  at 12 GHz when the bias voltage ranges from 0 V to 120 V.

Oliveira et al. [20] developed a project to control the gain and directivity of a circular patch UWB antenna. The cross-dipole RFSS has a PIN diode attached to each edge of the cross-dipole. When the diodes are in the OFF state, there is no current flowing between the elements. Thus, the RFSS will behave as a cross-dipole array with a band-stop response. When the diodes are in the ON state, current flows through the elements and the RFSS will behave as square loops with a bandpass response.

Bousslama et al. [21] developed a simple dipole antenna with beam switching. The project consists of an active cylindrical FSS containing PIN diodes, divided into 10 equal columns. Antenna beam scanning is produced by toggling the PIN diodes between ON and OFF states. The antenna operates at 1.8 GHz with a maximum measured gain of 9.1 dBi. Reis et al. [22] presented a structure designed to operate at 3.6 GHz (5G New Radio (NR) frequency band 1 (FR1) band n78), with low visual impact in dense 5G scenarios. The transmitarray used is composed of square slit resonant unit cells loaded with varactors. The antenna has the ability to direct the beam in a defined range of  $0^\circ$  and  $20^\circ$ , both in the azimuth plane and in the elevation plane. The proposed antenna features 13.9 dBi of gain and 100 MHz of bandwidth.

In this scenario, this paper presents an FSS as a reconfigurable superstrate applied to a dipole antenna for 5G NR, specifically in the 3.5 GHz frequency band, allowing the radiation pattern to be electronically redirected, which is confirmed by simulated and experimental results. It is worth noting

that ideal cases were considered, in which the ON and OFF states of the diodes were replaced by short circuits and gaps, respectively. After this Introduction, the FSS is described in Section II. The four arms star geometry is resented in Section III. In Section IV numerical and measured results are shown, including a detailed description of the manufacturing and measurement processes. Furthermore, the results are analyzed, verifying the redirection of the radiation pattern. Conclusions are commented in Section V.

## II. FREQUENCY SELECTIVE SURFACES (FSS)

The Frequency Selective Surfaces (FSS) are generally defined as planar structures that exhibit similar behavior to electromagnetic filters. These structures are designed to reflect or be transparent to electromagnetic waves. This behavior is determined according to the type of element used in the array, either patch (band-stop) or aperture (band-pass). In addition to the type of element, parameters such as thickness ( $h$ ), relative permittivity ( $\epsilon_r$ ) of the substrate, structure dimensions, element geometry, and its periodicity also influence the frequency response of the FSS [23]-[25], as shown in Fig.1.

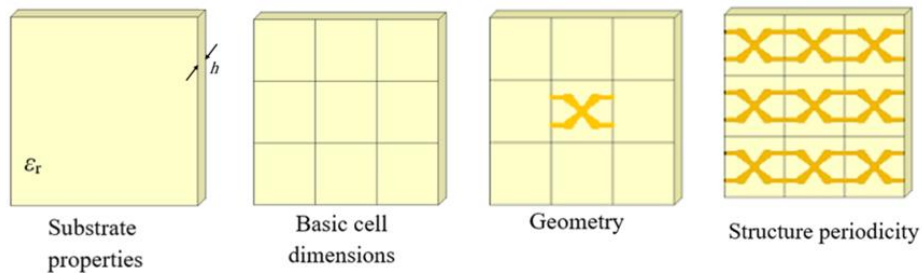


Fig. 1. Parameters that affect the FSS frequency response [26].

The FSSs have been a relevant topic of study in the last six decades due to their wide applications in microwave engineering [25]. FSS designs have been used in reflector antennas. [27], radomes [28],[29], radar cross section (RCS) reduction [30],[31], smart walls [32],[33], reconfigurable antennas [34],[35], electromagnetic interference protection [36], and absorber FSS [37]-[39], among others.

The factors that have sparked the interest of researchers in using FSS projects are the low manufacturing cost, reduced weight and volume, flexibility in the design of its unit cell, high capacity for integration with other circuit parts, and operation in several frequency bands, ranging from microwave to terahertz. This makes it possible to implement FSS in several telecommunications systems [25].

The disadvantages associated with FSS designs are few. Among them, the versatility in the design of the basic element geometry has a large electrical length, leading to an infinite variety of combinations. However, certain geometries do not have angular stability affecting the performance of the FSS. Fabrication of some FSS designs can be more complicated and the implementation of multiple layers can lead to an increase in volume and fabrication cost to achieve the desired result. Researchers are always looking for new methodologies to miniaturize and reduce the structural complexity to facilitate the fabrication and manufacture of FSSs [40].

One of the FSS applications that has drawn the attention of scholars is the development of more efficient antennas that can improve the transmission capacity of systems, directing the electromagnetic signal, favoring better use of the spectrum, and preventing the signal from being radiated in unwanted directions [10]-[12]. One way to direct the radiation pattern is to use the FSS as a superstrate, aiming to achieve the desired radiation characteristics [41]-[44]. In this context, the FSS can be electronically reconfigured, allowing one or more antenna operation characteristics to be changed (resonance frequency, radiation pattern, bandwidth, and polarization), making telecommunications systems more efficient, both from an energy point of view, as well as in terms of communication quality [45], [46]. Thus, the reduced cost, ease of implementation, and integration make the use of FSS as a reconfigurable superstrate an interesting feature for 5G NR networks [13].

### III. FOUR ARMS STAR GEOMETRY

The FSS based on the four arms star geometry was introduced in [47], [48] and presents attractive characteristics for several applications, including reconfiguration [26], [49]. The project starts with a unit cell with dimensions  $W_x$  and  $W_y$ , as shown in Fig. 2 (a). After it is added a conventional rectangular patch, with dimensions  $L_x$  and  $L_y$ , and a switching area with dimensions  $S_x$  and  $S_y$ , located in the center of the patch. The dimensions of the star's arms are defined by  $L_x$ ,  $L_y$  (same patch dimensions),  $dx$ ,  $dy$  (spacing from triangular gap to vertex of rectangular patch), and subsequently, diagonals are drawn from the ends of the star arms to the opposite corner of the switching point Fig. 2 (b). Finally, the part of the metallization layer that does not constitute the four arms star is removed and the desired structure is obtained, Fig. 2 (c). To insert a switching element, such as a PIN diode, a gap is introduced at the switching point, separating the lower and upper arms, Fig. 2 (d) [43]-[45]. As ideal cases were used, the bias lines were not used.

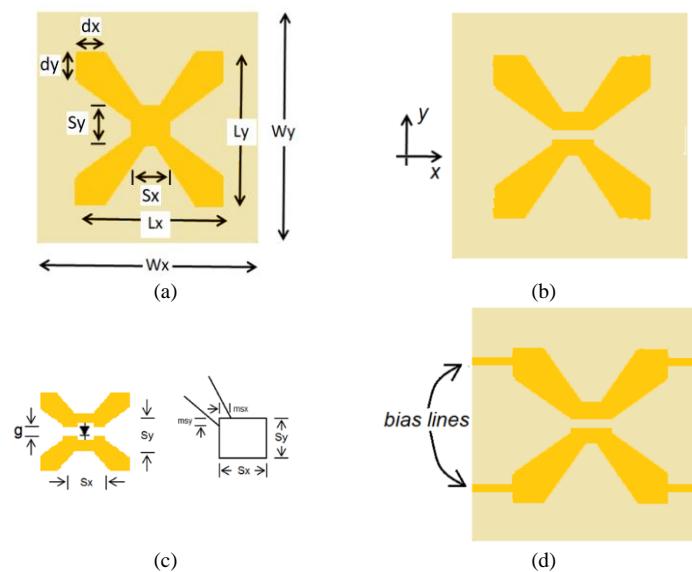


Fig. 2. Four arms star geometry step by step [26]. (a) Geometry dimensions, without gap; (b) Geometry with gap; (c) Gap details; (d) Geometry with gap and bias lines.

Without the gap, the FSS resonant frequency can be approximately determined by (1), with good

results, principally for  $h \ll \lambda_0$ , [29], [30].

$$f_{res}(GHz) = \frac{0.3}{2L_{eff}} \quad (1)$$

In which  $L_{eff} = Lx + Ly$ , with  $L_{eff}$  in meters. Considering the  $y$  polarization, with the gap and the bias lines, the resonant frequency,  $f_{res-gb}$ , can be estimated by (2), [27].

$$1.5f_{res} \leq f_{res-g}(GHz) \leq 2.0f_{res} \quad (2)$$

#### IV. NUMERICAL AND MEASURED RESULTS

Simulations were performed using ANSYS Electronics Desktop, specifically HFSS for 3D modeling of structures with the finite element method. The software was used for the simulations of the antenna, the unit cell, and the structure formed by the antenna and FSS acting as a superstrate. In all simulations, used low-cost substrate FR-4 with  $\epsilon_r = 4.4$ ,  $h = 1.6$  mm and loss tangent ( $\tan(\delta)$ ) equal to 0.02. The prototypes were fabricated using printed circuit techniques on an adhesive and it is attached to the substrate surface. Then, the metallic surface that is not part of the FSS is removed by corrosion in iron perchloride. The aforementioned measurements were conducted at the GTEMA-IFPB Microwave Laboratory using a VNA Agilent E5071C in combination with a double ridge guide A. H. Systems, model SAS-571 (ranging from 700 MHz to 18 GHz) [50], as depicted in Fig. 3. Although the measurements were not carried out in an anechoic chamber, it was possible to verify the redirection of the antenna radiation pattern.

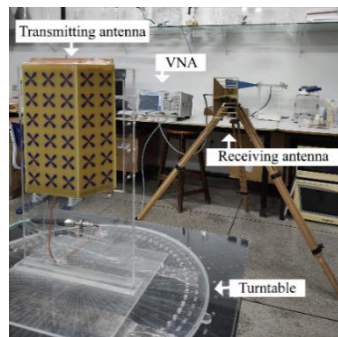


Fig. 3. Measurement setup.

The Fig. 4 provides the dimensions of the geometry used in the experiment. The utilized FSS is a band-reject type, where the metal is represented in orange and the dielectric is represented in beige. Note that ideal cases were considered, where the ON, Fig. 4 (a), and OFF states of the diodes were replaced by short circuits and gaps, Fig. 4(b), respectively.

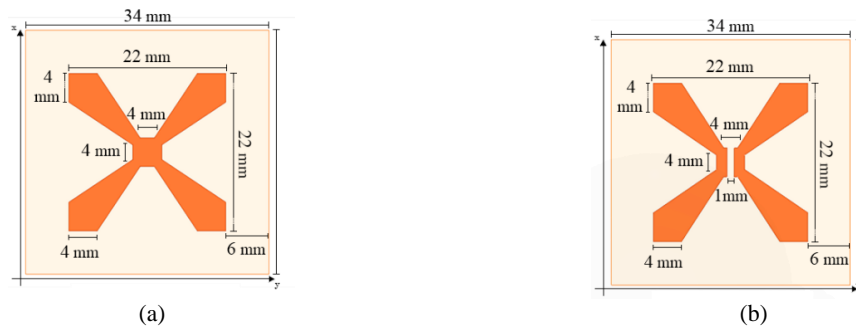


Fig. 4. Proposed structure. (a) Cell ON, (b) Cell OFF.

The resonant frequency calculated using equation (1) for the ideal PIN diode ON state is 3.41 GHz, which is in good agreement with the simulated resonant frequency of 3.54 GHz. In Fig. 5 (a), the frequency response for the ideal FSS with the PIN diode ON state is shown. Since the structure is symmetric, only the result for  $x$  polarization is presented. Fig. 5 (b) illustrates the frequency response of the unit cell for the OFF state, where the PIN diode is represented by a gap, for both  $x$  and  $y$  polarizations. It is worth noting that the presence of the gap does not seem to significantly impact the frequency response for the  $y$  polarization. However, for  $x$  polarization at 3.545 GHz, the unit cell frequency response experiences a variation of at least 30 dB, ranging from -31 dB to -1 dB. This variation is leveraged to reconfigure the antenna, making it a useful feature to have.

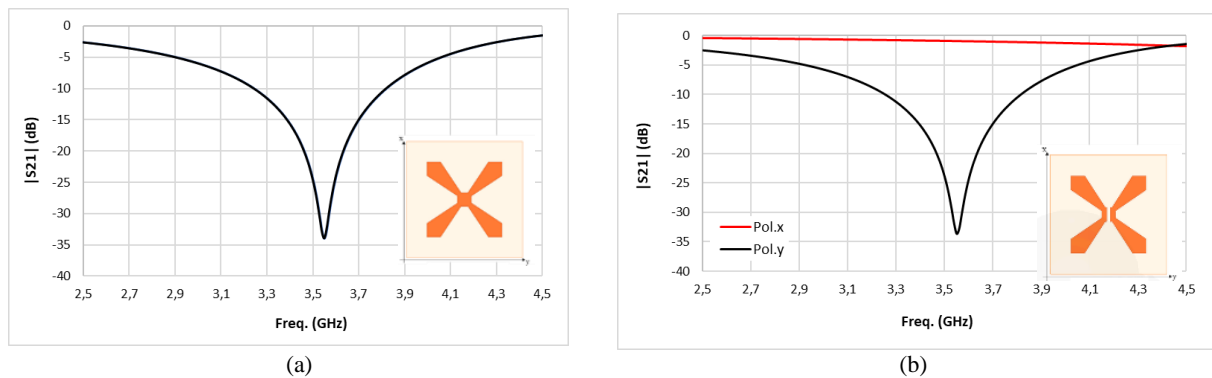


Fig. 5. Frequency response, FSS. (a) Ideal ON state, (b) Ideal OFF state.

### A. Dipole antenna

The antenna was fabricated using a semi-rigid cable from the brand Huber-Suhner, model EZ141TP [51], of 30 cm, with SMA connectors at the ends. The cable was split for the fabrication of the poles, one of the poles being formed by the central conductor and the other formed by removing a part of the central conductor, soldered to the outer conductor, with a total length of 42 mm. The symmetry of the dipole is not ideal, which is evident from Fig. 6 displaying the frequency response of the fabricated dipole. However, it is worth noting that the simulation predicted a resonance frequency of 3.47 GHz, which is a good approximation when compared to the measured value of 3.51 GHz.

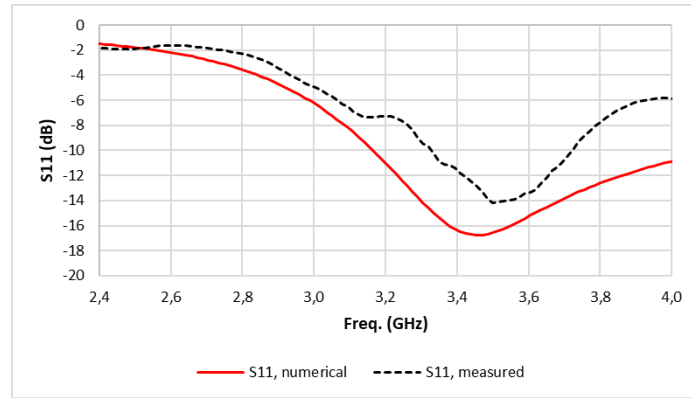


Fig. 6. Frequency response, isolated dipole.

### B. Proposed Structure

The structure that has been developed is depicted in Fig. 7. The superstrate is made up of 7 rows of unit cells, each numbered from 1 to 7. It is possible to control each row independently by switching the unit cells from an ON state to an OFF state and vice versa.

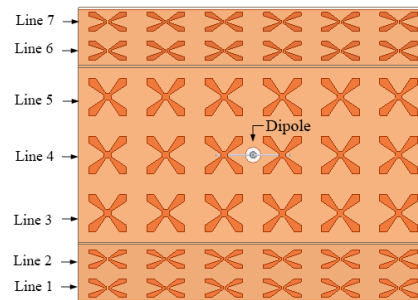


Fig. 7. Line identification.

The proposed antenna is shown in Figs. 8 (a), simulated antenna, and 8 (b), fabricated antenna. When there is a gap, the OFF state, the dipole, and therefore the electric field is perpendicular to it, which allows taking advantage of the variation of its frequency response when compared to the ON state.

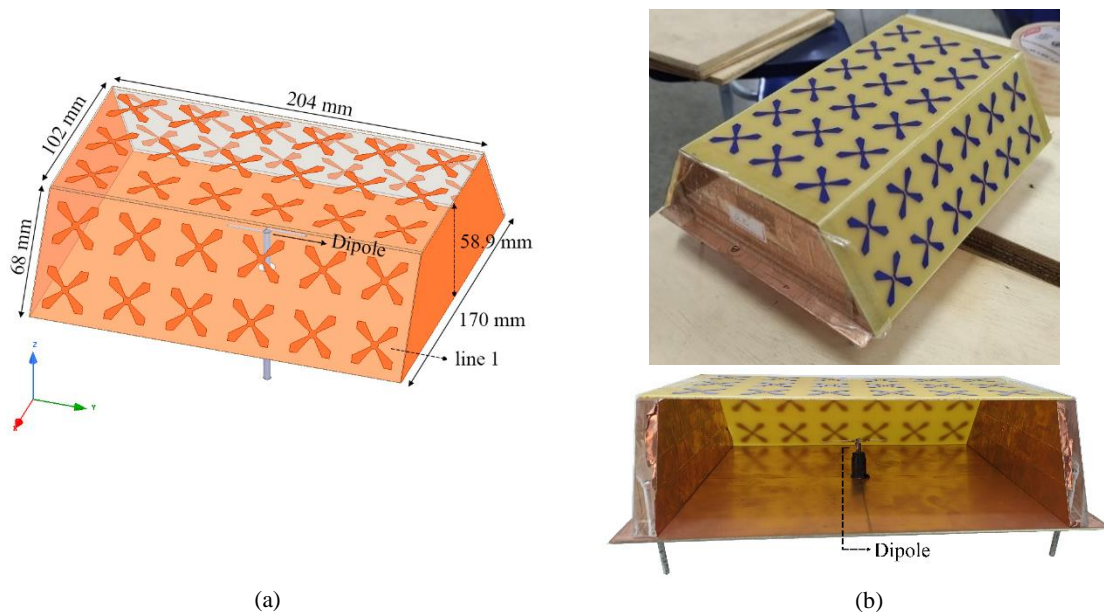


Fig. 8. Proposed antenna. (a) Simulated antenna, (b) Fabricated antenna.

The radiation pattern measurements were performed in the  $xz$  plane, with the dipole in the  $y$  direction, Fig. 9, with  $\phi = 0^\circ$  and  $\theta$  ranging from  $0^\circ$  to  $360^\circ$ , at intervals of  $5^\circ$ . For co-polarization, the receiving antenna is polarized in the same direction as the dipole. For the cross-polarization measurement, the receiving antenna is polarized in the  $x$  direction.

The experimental setup initially involves measuring the value of  $S_{21}$  in dB for each angular position, which results in a radiation pattern as shown in Fig. 10 (a). These measured results are then normalized with respect to the maximum value obtained during the measurement, specifically for the co-polarization - VV. This normalized value is then equated to the maximum gain obtained during the simulation. The resulting normalized diagram is presented in Fig. 10 (b), where the values from Fig. 10 (a) are normalized to a maximum gain of 9.93 dBi.

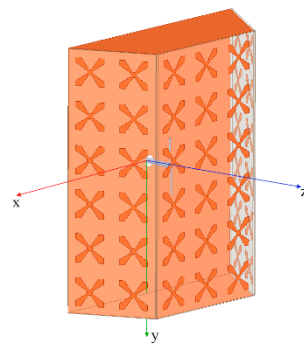


Fig. 9. Measuring plan for fabricated prototype.

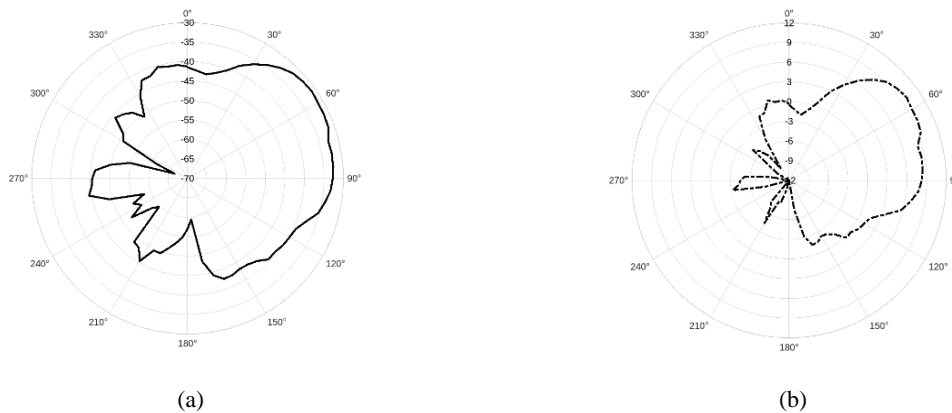


Fig. 10. Radiation pattern. (a) Measured, without normalization; (b) Measured, normalized

Table I shows the values of  $S_{11}$ , the maximum values of  $S_{21}$  for co-polarization, and for the same angular position, the value corresponds to cross-polarization, for all three analyzed configurations. These values give an idea of the isolation between polarizations.

TABLE I. SUMMARY OF PROPOSED CONFIGURATIONS.

| Configuration     | $S_{11}$ (dB) | $S_{21}$ (dB) VV | $S_{21}$ (dB) VH | Gain (dBi) |
|-------------------|---------------|------------------|------------------|------------|
| All lines OFF     | -9.61         | -36.50           | -59.07           | 4.79       |
| All lines ON      | -11.00        | -36.50           | -63.98           | -1.67      |
| Lines 1 and 2 OFF | -15.47        | -31.06           | -46.89           | 9.93       |
| Lines 6 and 7 OFF | -9.00         | -32.19           | -53.46           | 10.16      |

The upcoming analysis will take each case into account individually. In Figs. 11 (a) and (b), the simulation and measurement outcomes, respectively, are presented for the configuration with all lines switched OFF. In this scenario, the FSS is allowing the signal to pass through, as illustrated in Fig. 5 (b). The outcomes of the measurements were normalized with  $-36.5$  dB and  $4.79$  dBi, as shown in Table I.

The Fig. 12 (a) displays the 3D radiation pattern for realized gain, where the maximum gain value is  $7.7$  dBi. In Fig. 12 (b) the diagram is plotted over the structure, and it can be observed that the maximum gain value exceeds the value of  $4.79$  dBi. This is due to the plane used for the cut in the 3D diagram.

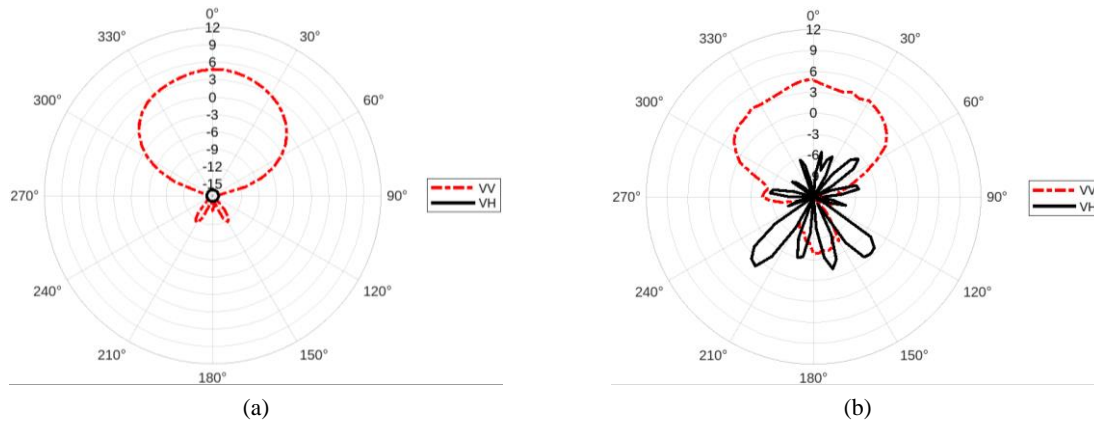


Fig. 11. Radiation pattern, all lines OFF. (a) Simulated, (b) Measured.

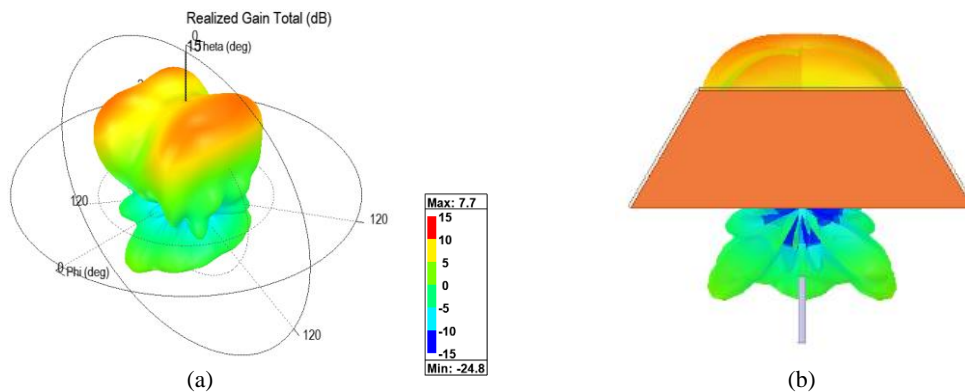


Fig. 12. Radiation pattern, 3D, all lines OFF. (a) Gain realized, (b) Side view.

In Fig. 13, it can be observed that when all lines are turned ON, the FSS effectively blocks the entire signal. The results of simulations, Fig. 13 (a), and measurements, Fig. 13 (b), are presented, with the measured results being normalized using values of  $-36.5$  dB and  $-1.67$  dBi as shown in Table I. Additionally, Fig. 14 depicts the 3D radiation pattern for realized gain, with a maximum value of  $1.6$  dBi, Fig. 14 (a), as well as the diagram plotted on the structure, Fig. 14 (b).

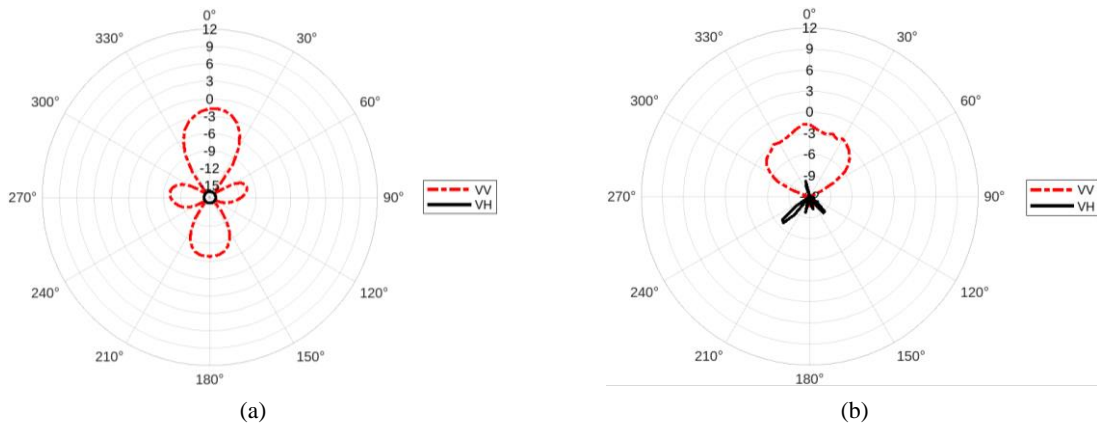


Fig. 13 – Radiation pattern, all lines ON. (a) Simulated, (b) Measured.

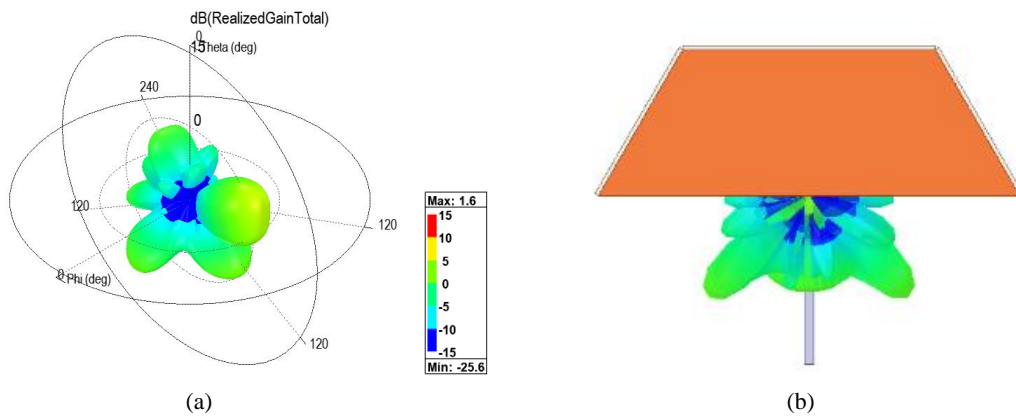


Fig. 14. Radiation pattern, 3D, all lines ON. (a) Gain realized, (b) Side view.

Fig. 15 (a) shows the simulated results for the configuration with lines 1, 2 OFF. The measured results, presented in Fig. 15 (b), were normalized with -31.06 dB and 9.93 dBi, as shown in Table I.

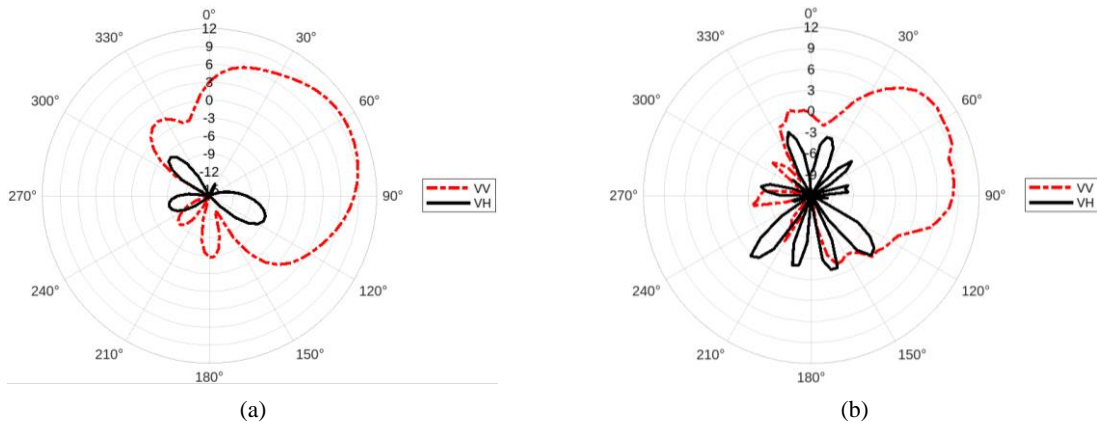


Fig. 15. Radiation pattern, lines 1,2 OFF. (a) Simulated, (b) Measured.

Fig. 16 (a) shows the 3D radiation pattern, for realized gain, with a maximum value of 9.4 dBi. In Fig.16 (b) the diagram is plotted over the structure.

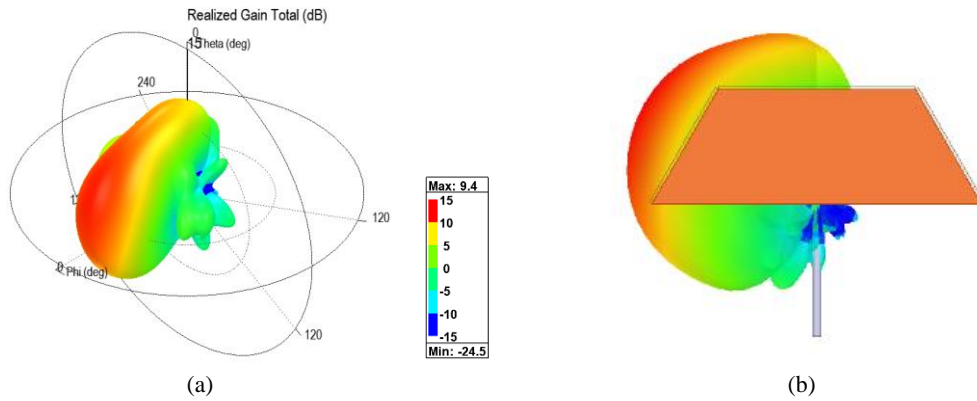


Fig. 16. Radiation pattern, 3D, lines 1,2 OFF. (a) Realized gain total, (b) Side view.

In Figs. 17 (a) and 17 (b), simulated and measured results, respectively, are presented for the configuration with lines 6, 7 OFF. The measured results were normalized with -32.19 dB and 10.16 dBi, as shown in Table I.

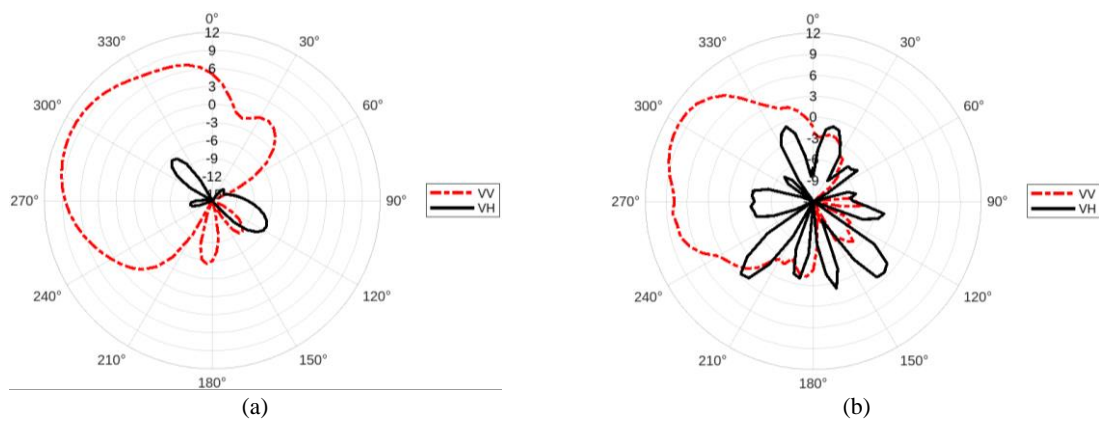


Fig. 17. Radiation pattern, lines 6,7 OFF. (a) Simulated, (b) Measured.

Fig. 18 (a) shows the 3D radiation pattern, for realized gain, with a maximum value of 9.5 dBi. Fig. 18 (b) the diagram is plotted over the structure.

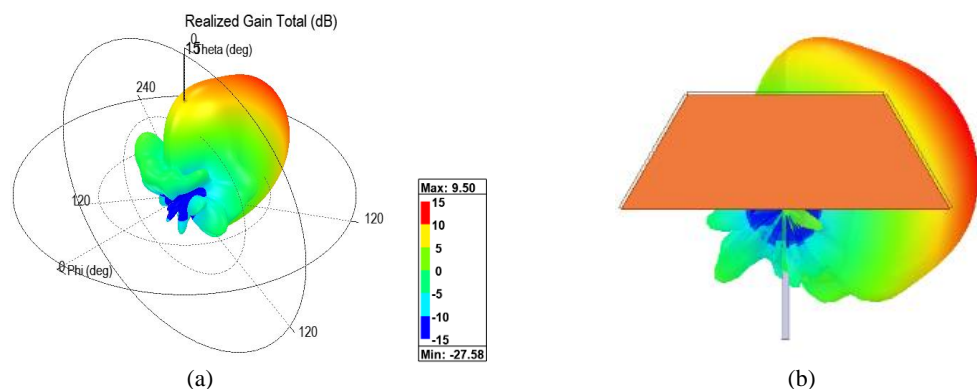


Fig. 18. Radiation pattern, 3D, lines 6,7 OFF. (a) Gain realized, (b) Side view.

In Figs. 19 (a) and 19 (b), simulated and measured results, respectively, the radiation patterns for different configurations are compared: all lines OFF, lines 1 and 2 OFF, and lines 6 and 7 OFF. It can be verified that for lines 6 and 7 in the OFF configuration, the antenna with the superstrate redirects the

radiation diagram, with a maximum gain for  $\theta = -60^\circ$ . Note that this configuration is symmetric to the configuration with lines 1 and 2 OFF, with a maximum gain for  $\theta = 60^\circ$ .

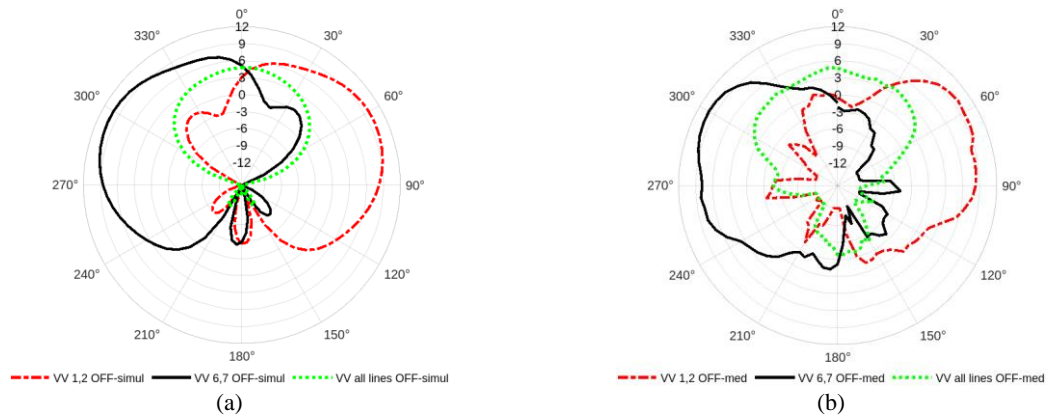


Fig. 19. Radiation pattern comparison, 1, 2 OFF, 6,7 OFF and all lines OFF. (a) Simulated, (b) Measured.

Table II summarizes the results obtained with all lines OFF, lines 1 and 2 OFF, and lines 6 and 7 OFF. The maximum total gain, maximum realized gain, and maximum gain for  $\phi = 0^\circ$ , and the respective  $\theta$  value, are shown.

TABLE II - SUMMARY OF RESULTS FOR ALL LINES OFF, LINES 1 AND 2 OFF, LINES 6 AND 7 OFF.

| Configuration     | Gain max. total (dBi) | Gain max. realiz. (dBi) | Gain max. (dBi), $\phi=0^\circ$ | Max. sim. value, $\theta$ | Max. meas. value, $\theta$ |
|-------------------|-----------------------|-------------------------|---------------------------------|---------------------------|----------------------------|
| Lines 1 and 2 OFF | 10.2                  | 9.4                     | 9.93                            | $60^\circ$                | $55^\circ$                 |
| Lines 6 and 7 OFF | 10.27                 | 9.5                     | 10.16                           | $-65^\circ$               | $-60^\circ$                |
| All lines OFF     | 8.1                   | 7.7                     | 4.79                            | $0^\circ$                 | $0^\circ$                  |

Aiming to illustrate other possibilities for reconfiguration, Fig. 20 (a) presents numerical results for lines 2, 3 and 4 OFF, and lines 4,5 and 6 OFF. In Fig. 20 (b), results are also presented for lines 2 and 3 OFF, and lines 5 and 6 OFF. With these results it is possible to see that the proposed structure allows different intermediate angles for directing the radiation diagram.

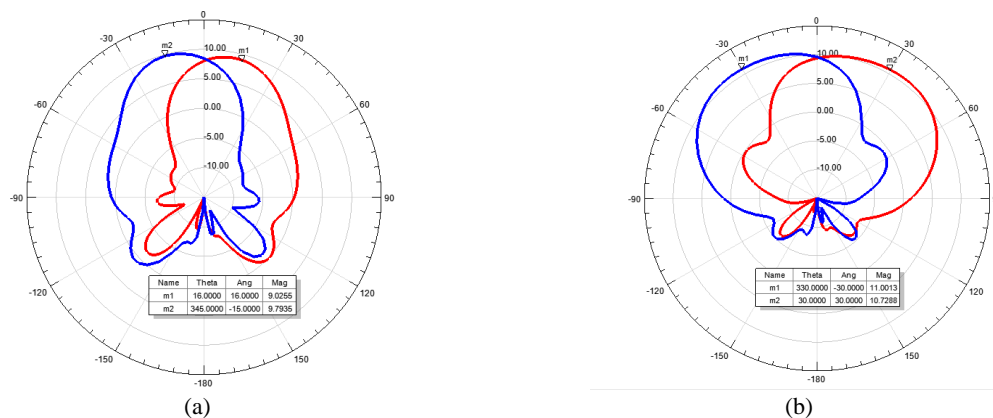


Fig. 20. Numerical results for intermediate angles for directing the radiation diagram. (a) Lines 2, 3 and 4 OFF (red), lines 4,5 and 6 OFF (blue); (b) Lines 2 and 3 OFF (red), lines 5 and 6 OFF (blue).

## V. CONCLUSION

In this paper, a band-stop FSS was used as reconfigurable superstrate and applied to a dipole antenna. The FSS was designed based on the four arms star geometry. The antenna plus FSS intended for use in 5G NR technology. The simulation and fabrication of the dipole antenna were carried out successfully. The frequency response of the reconfigurable FSS showed a variation of approximately 30 dB when switching between the OFF and ON states. This variation was used to reconfigure the antenna for the analyzed frequency, 3.545 GHz. The developed structure was analyzed in three different configurations. In all lines OFF configuration, when the FSS allows the signal to pass through, it was observed that the antenna with the superstrate achieved maximum gain for  $\phi = 0^\circ$ ,  $\theta = 0^\circ$ . As expected, for the all ON configuration, when the FSS blocks the signal, the radiation for the same angular position was significantly lower. For lines 1 and 2 in the OFF configuration, it was found that the antenna with the superstrate redirected the radiation pattern, and it had a maximum gain at  $\theta = 60^\circ$ , for  $\phi = 0^\circ$ . On the other hand, for lines 6 and 7 in the OFF configuration, it was observed that the redirection of the radiation pattern occurred with a maximum gain at  $\theta = -55^\circ$ , for  $\phi = 0^\circ$ . When comparing the last two configurations, it was noticed that the redirection of the radiation pattern was up to  $\pm 55^\circ$  for the frequency, a very attractive result for 5G NR technology.

## REFERENCES

- [1] A. Osseiran, F. Boccardi, V. Braun, K. Kusume, P. Marsch, M. Maternia, O. Queseth, M. Schellmann, H. Schotten, H. Taoka, H. Tullberg, M. A. Uusitalo, B. Timus, and M. Fallgren, "Scenarios for 5G mobile and wireless communications: the vision of the METIS project," *IEEE Communications Magazine*, vol. 52, no. 5, pp. 26-35, 2014.
- [2] L. Zhang, A. Ijaz, P. Xiao, and R. Tafazolli, "Multi-Service System: An Enabler of Flexible 5G Air Interface," *IEEE Communications Magazine*, vol. 55, no. 10, pp. 152-159, 2017.
- [3] Y. Niu, Y. Li, D. Jin, L. Su, and A. V. Vasilakos, "A survey of millimeter wave communications (mmWave) for 5G: opportunities and challenges," *Wireless Networks*, vol. 21, no. 8, pp. 2657-2676, 2015.
- [4] W. Chen, G. Lv, X. Liu, D. Wang and F. M. Ghannouchi, "Doherty PAs for 5G Massive MIMO: Energy-Efficient Integrated DPA MMICs for Sub-6-GHz and mm-Wave 5G Massive MIMO Systems," in *IEEE Microwave Magazine*, vol. 21, no. 5, pp. 78-93, 2020.
- [5] S. Shinjo, K. Nakatani, K. Tsutsumi and H. Nakamizo, "Integrating the Front End: A Highly Integrated RF Front End for High-SHF Wide-Band Massive MIMO in 5G," in *IEEE Microwave Magazine*, vol. 18, no. 5, pp. 31-40, 2017.
- [6] S. Chen, S. Sun, Q. Gao and X. Su, "Adaptive Beamforming in TDD-Based Mobile Communication Systems: State of the Art and 5G Research Directions," *IEEE Wireless Communications*, vol. 23, no. 6, pp. 81-87, 2016.
- [7] F. Chen, X. Li, Y. Zhang and Y. Jiang, "Design and implementation of initial cell search in 5G NR systems," in *China Communications*, vol. 17, no. 5, pp. 38-49, 2020.
- [8] J. Liu *et al.*, "Initial Access, Mobility, and User-Centric Multi-Beam Operation in 5G New Radio," in *IEEE Communications Magazine*, vol. 56, no. 3, pp. 35-41, 2018.
- [9] Anatel. [Online] Available: <https://www.gov.br/anatel/pt-br/assuntos/5G/leilao-de-espectro-5g>. [Acesso em 07 janeiro 2022].
- [10] D. Sievenpiper, J. Schaffner, R. Loo, G. Tandon, S. Ontiveros and R. Harold, "A tunable impedance surface performing as a reconfigurable beam steering reflector," *IEEE Transactions on Antennas and Propagation*, vol. 50, no. 3, pp. 384-390, 2002.
- [11] H. Kawakami and T. Ohira, "Electrically steerable passive array radiator (ESPAR) antennas," *IEEE Antennas and Propagation Magazine*, vol. 47, no. 2, pp. 43-50, 2005.
- [12] N. C. Karmakar and M. E. Bialkowski, "A beam-forming network for a circular switched-beam phased array antenna," *IEEE Microwave and Wireless Components Letters*, vol. 11, no. 1, pp. 7-9, 2001.
- [13] D. McGrath, "Planar Three-Dimensional Constrained Lenses," *IEEE Transactions on Antennas and Propagation*, vol. 34, no. 1, pp. 46-50, 1986.
- [14] J. R. Reis, M. Vala and R. F. S. Caldeirinha, "Review Paper on Transmitarray Antennas," in *IEEE Access*, vol. 7, pp. 94171-94188, 2019.
- [15] J. Y. Lau, "Reconfigurable Transmitarray Antennas," Ph.D. dissertation, University of Toronto, 2012.
- [16] L. D. Palma, "Reconfigurable Transmitarray Antennas at Millimeter-Wave Frequencies," Ph.D., Université de Rennes 1, 2015.

- [17] S. Hum and J. Perruisseau-Carrier, "Reconfigurable Reflectarrays and Array Lenses for Dynamic Antenna Beam Control: A Review," *IEEE Transactions on Antennas and Propagation*, vol. 62, no. 1, pp. 183–198, 2014.
- [18] A. Pirhadi, F. Keshmiri and M. Hakkak, "Design of dual-band low profile high directive EBG resonator antenna, using single layer frequency selective surface (FSS) superstrate," *2006 IEEE Antennas and Propagation Society International Symposium*, Albuquerque, NM, Julho 2006, pp. 3005-3008.
- [19] M. Sazegar et al., "Beam Steering Transmitarray Using Tunable Frequency Selective Surface with Integrated Ferroelectric Varactors," in *IEEE Transactions on Antennas and Propagation*, vol. 60, no. 12, pp. 5690-5699, 2012.
- [20] M. R. T. Oliveira et al., "RFSS based on cross dipole or grid using PIN diode," *Microwave and Optical Technology Letters*, v. 59, p. 2122-2126, 2017.
- [21] M. Bouzlama et al., "Beam-Switching Antenna with a New Reconfigurable Frequency Selective Surface," in *IEEE Antennas and Wireless Propagation Letters*, vol. 15, pp. 1159-1162, 2016, doi: 10.1109/LAWP.2015.2497357.
- [22] J. R. Reis et al. "Metamaterial-inspired Flat-Antenna Design for 5G Small-cell Base-Stations Operating at 3.6 GHz," *2020 12th International Symposium on Communication Systems, Networks and Digital Signal Processing (CSNDSP)*, 2020, pp. 1-5, doi: 10.1109/CSNDSP49049.2020.9249497.
- [23] B.A. Munk. "Frequency Selective Surfaces: Theory and Design", Wiley Online Library: Hoboken, NJ, USA, 2000.
- [24] J. C. Vardaxoglou, "Frequency Selective Surfaces: Analysis and Design", Research Studies Press: Boston, MA, USA, 1997.
- [25] R. S Anwar, L. Mao, H. Ning. "Frequency Selective Surfaces: A Review". *Applied Sciences*. 2018; 8(9):1689. <https://doi.org/10.3390/app8091689>.
- [26] T. da S. Evangelista, et al. "A Reconfigurable Frequency Selective Surface for Wi-Fi Application". *Journal of Microwaves, Optoelectronics and Electromagnetic Applications*, v. 22, p. 33-46, 2023.
- [27] J. A. Arnaud, F. A. Pelow, "Resonant-grid quasi-optical diplexers", *The Bell System Technical Journal*, . J. 1975, 54, 263–283.
- [28] A. A. Omar and Z. Shen, "Thin 3-D bandpass frequency-selective structure based on folded substrate for conformal radome applications," *IEEE Transactions on Antennas and Propagation*, vol. 67, no. 1, pp. 282–290, 2019.
- [29] B. Sangeetha, G. Gulati, R. U. Nair, and S. Narayan, "Design of airborne radome using swastika-shaped metamaterial-element based FSS," *2016 IEEE Annual India Conference (INDICON)*, 2016, pp. 1–5.
- [30] M. Pazokian, N. Komjani, and M. Karimipour, "Broadband rcs reduction of microstrip antenna using coding frequency selective surface," *IEEE Antennas and Wireless Propagation Letters*, vol. 17, no. 8, pp. 1382–1385, 2018.
- [31] H. B. Baskey and M. J. Akhtar, "Design of flexible hybrid nanocomposite structure based on frequency selective surface for wideband radar cross section reduction," *IEEE Transactions on Microwave Theory and Techniques*, vol. 65, no. 6, pp. 2019–2029, 2017.
- [32] S. Habib, G. I. Kiani, and M. F. U. Butt, "Interference mitigation and wlan efficiency in modern buildings using energy saving techniques and FSS," *2016 IEEE International Symposium on Antennas and Propagation (APSURSI)*, 2016, pp. 965–966.
- [33] M. Gustafsson, A. Karlsson, A. Rebelo, and B. Widenberg, "Design of frequency selective windows for improved indoor outdoor communication", *IEEE Transactions on Antennas and Propagation*, vol. 54, no. 6, pp. 1897–1900, 2006.
- [34] D. F. Mamedes, A. G. Neto, and J. Bornemann, "Reconfigurable corner reflector using pin-diode-switched frequency selective surfaces," *2020 IEEE International Symposium on Antennas and Propagation and North American Radio Science Meeting*, 2020, pp. 127–128.
- [35] S. M. Mahmood and T. A. Denidni, "Pattern-reconfigurable antenna using a switchable frequency selective surface with improved bandwidth," *IEEE Antennas and Wireless Propagation Letters*, vol. 15, pp. 1148–1151, 2016.
- [36] D. Li, T. -W. Li, E. -P. Li and Y. -J. Zhang, "A 2.5-D Angularly Stable Frequency Selective Surface Using Via-Based Structure for 5G EMI Shielding," *IEEE Transactions on Electromagnetic Compatibility*, vol. 60, no. 3, pp. 768-775, 2018, doi: 10.1109/TEMC.2017.2748566.
- [37] T. C Areias et al. "Frequency Selective Surface Microwave Absorber for WLAN Applications", *Journal of Communication and Information Systems*, v. 35, n. 1, p. 208, 2020.
- [38] D. Kundu, A. Mohan and A. Chakrabarty, "Design of a Conductive FSS based Ultrathin Absorber Using Impedance Analysis Method of Equivalent Circuit Model," *2018 IEEE Indian Conference on Antennas and Propagation (InCAP)*, Hyderabad, India, 2018, pp. 1-4, doi: 10.1109/INCAP.2018.8770792.
- [39] J. da S. Souza, A. J. R. Serres and A. G. Neto, "A Novel FSS Absorber for 5 GHz WLAN Applications," *2022 IEEE International Symposium on Antennas and Propagation and USNC-URSI Radio Science Meeting (AP-S/URSI)*, Denver, CO, USA, 2022, pp. 1248-1249, doi: 10.1109/AP-S/USNC-URSI47032.2022.9886032.
- [40] K. Katoch; N. Jaglan; S. D. Gupta. "A review on frequency selective surfaces and its applications", in: *2019 International Conference on Signal Processing and Communication (ICSC)*. IEEE, 2019. p. 75-81.
- [41] R. Mittra, and D. Lee, "Analysis of a frequency selective surface radome located in close proximity of a phased array antenna", *IEEE Antennas and Propagation Society International Symposium*, vol. 4, pp.370-373, 2001.
- [42] Yueh-Lin Tsai, Ruey-Bing Hwang and Yu-De Lin, "A reconfigurable beam-switching antenna base on active FSS," *15 International Symposium on Antenna Technology and Applied Electromagnetics*, Toulouse, 2012, pp. 1-4.
- [43] A. Edalati, T. A. Denidni, "High-gain reconfigurable sectoral antenna using an active cylindrical FSS structure." *IEEE Transactions on Antennas and Propagation*, vol. 59, no. 7, pp. 2464-2472, 2011.
- [44] I. Y. Tarn and S. J. Chung, "A novel pattern diversity reflector antenna using reconfigurable frequency selective reflectors." *IEEE Transactions on Antennas and Propagation*, vol. 57, no. 10, pp. 3035-3042, 2009.
- [45] R. Gonçalves e P. Pinho, "Antena impressa reconfigurável de pequena dimensão para dispositivos móveis" 6º Congresso do Comitê Português da URS, Lisboa, 2012.

- [46] R. S. G. Nabi, “Antenas Impressas Activas Multibanda para Comunicações Móveis.” Dissertação de Mestrado em Engenharia Eletrônica e Telecomunicações, ISEL, Lisboa, 2007.
- [47] I. S. S. Lima, “Characterization of FSS with Four Arms Star Geometry,” in *Portuguese*, “Caracterização de FSS com Geometria em Forma de Estrela de Quatro Braços,” Master thesis, PPGEE, Federal Institute of Paraíba, João Pessoa, Paraíba, Brazil, 2014.
- [48] L. C. M. de Moura, “Characterization of FSS with Slot Type Four Arms Star Geometry,” in *Portuguese*, “Caracterização de FSS com Geometria Estrela de Quatro Braços Tipo Fenda”, Master thesis, PPGEE, Federal Institute of Paraíba, João Pessoa, Paraíba, Brazil, 2015.
- [49] D.F. Mamedes, A. G. Neto, J. C. e Silva, and J. Bornemann, “Design of reconfigurable frequency- selective surfaces including the PIN diode threshold region”. *IET Microwaves, Antennas & Propagation*, vol. 12, pp. 1483-1486, 2018. <https://doi.org/10.1049/iet-map.2017.0761>.
- [50] SAS-571 datasheet. [Online] Available: [https://www.ahsystems.com/datasheets/SAS571\\_Horn\\_Antenna\\_Datasheet.pdf](https://www.ahsystems.com/datasheets/SAS571_Horn_Antenna_Datasheet.pdf) [acessado em 08 de janeiro de 2022].
- [51] Huber+Suhner, EZ141 Datasheet [Online] Available: [https://br.mouser.com/ProductDetail/HUBER%2BSUHNER/24\\_N-50-3-51-19](https://br.mouser.com/ProductDetail/HUBER%2BSUHNER/24_N-50-3-51-19) [https://br.mouser.com/ProductDetail/HUBER%2BSUHNER/24\\_N-50-3-51-19](https://br.mouser.com/ProductDetail/HUBER%2BSUHNER/24_N-50-3-51-19) [Acessado em 17 de janeiro de 2022].